Journal of Materials Chemistry C

Accepted Manuscript

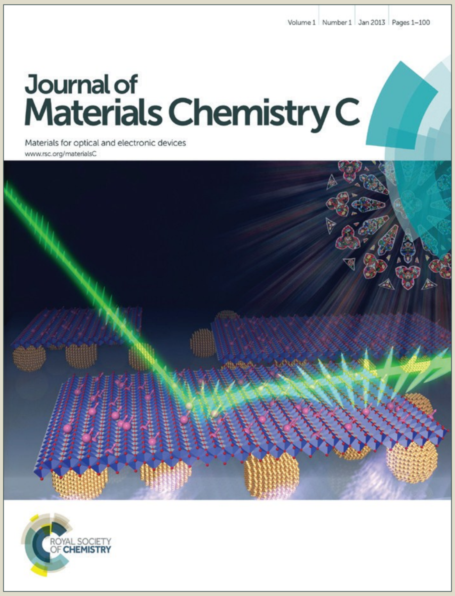

ROYAL SOCIETY
OF **CHEMISTRY**

www.rsc.org/materialsC

Journal Name

ARTICLE TYPE

Cite this: DOI: 10.1039/xxxxxxxxxx

Received Date
Accepted Date

DOI: 10.1039/xxxxxxxxxx

www.rsc.org/journalname

Magnetoelectric coupling and spin-induced electrical polarization in metal-organic magnetic chains

Marco Scarrozza,*[a] Paolo Barone,[a] Roberta Sessoli,[b] and Silvia Picozzi[a]

We explore by density functional calculations the possible variation of a magnetically induced electric polarization in the prototypical single-chain magnet CoPhOMe and related MnPhOMe, underlying a sizable magnetoelectric interaction with appealing perspectives in cross-coupled control of their magnetic and electric properties. We find that going from ferrimagnetic to ferromagnetic hypothetical configurations gives rise to a non-negligible electric polarization along the helices axis, estimated up to 0.100 μC/cm^2 and 0.065 μC/cm^2 for the Co- and Mn-based chains, respectively. Our analysis sheds light on the microscopic nature of the spin-induced electric polarization, showing that the dominant contribution is an isotropic exchange-driven mechanism, modulated by the relative alignment of the spin pairs between the $3d$-ions and the neighboring radicals. Moreover, we quantified the variation of the local electric dipoles produced by the local switching of the magnetic bondings along the chains, providing insight on the dipoles that may develop at the domain walls of the magnetic systems. Our theoretical prediction of spin-induced polarization and magnetoelectric coupling in metal-organic magnetic helices opens up interesting perspectives such as the modulation of their magnetization dynamics via electric fields.

1 Introduction

Multifunctional materials are attracting an ever increasing interest due to their obvious enhanced efficiency in integrating different functionalities within a single material, offering in addition the appealing possibility to control their physical properties via cross-coupling effects. One of the most celebrated examples in solid-state systems is that of magnetoelectric materials, where the magnetoelectric cross-coupling allows for an electric (magnetic) control and modulation of magnetic (electric) responses. Although the magnetoelectric effect has been long known[1,2], in the last two decades it has been the object of renewed interest and intense research due to its potential appeal for novel device applications[3,4]. Significant advances in the field have been achieved in the related class of multiferroics, i.e., materials displaying a coexistence of spontaneous magnetic and ferroelectric orderings[5,6]. Even though such a coexistence is not a necessary condition for the magnetoelectric coupling to exist, a subclass of multiferroic materials has been early on identified where ferroelectricity arises from magnetic order, implying a sizeable magnetoelectric coupling and in many cases anomalously large magnetoelectric effects[7–10].

Several microscopic mechanisms for such magnetically-induced electric polarization and magnetoelectric coupling have been devised thereafter, including exchange-striction mechanisms as well as purely electronic spin-dependent mechanisms. A necessary condition for the magnetically induced polarization to appear is the inversion-symmetry breaking, that can be induced by specific magnetic orders, typically realized in frustrated magnets; such symmetry breaking may manifest as a structural transition (magnetostrictive mechanisms) or it may occur in the magnetic electronic ground state without necessarily involving structural distortions. On very general grounds, three kinds of mechanisms are expected to lead to an electric dipole emerging from a pair of adjacent spin sites: a local intra-site mechanism, typically due to spin-orbit coupling (SOC) causing an anisotropic spin-dependent charge redistribution around each spin site[11–13], and two inter-site mechanisms where the spin-spin correlations can lead to the

---

[a] CNR SPIN, UOS L'Aquila, via Vetoio 10, 67100 Coppito, L'Aquila, Italy.
[b] Laboratory of Molecular Magnetism (LaMM), Dip.to di Chimica Ugo Schiff, Università degli Studi di Firenze & INSTM RU, via della Lastruccia 3-13, 50019 Sesto Fiorentino (FI), Italy.

appearance of a local dipole $\boldsymbol{P}$ in the spin dimer[14,15]. If the spin dimer possesses an inversion center, the only allowed inter-site mechanism predicts $\boldsymbol{P} \propto \boldsymbol{S}_1 \times \boldsymbol{S}_2$, i.e., the spin-induced electric polarization is proportional to the spin current originating from an antisymmetric spin configuration[16–18]. This spin-current – or inverse Dzyaloshinskii-Moriya – mechanism originates ultimately from the interplay of the atomic SOC and hybridization effects between spin sites, and it has been identified in many frustrated magnets displaying cycloidal spin orderings, despite the measured polarizations are typically small ($\lesssim 0.1 \mu C/cm^2$)[19–21]. On the other hand, a symmetric exchange-driven electric polarization $\boldsymbol{P} \propto \boldsymbol{S}_1 \cdot \boldsymbol{S}_2$ may arise if the spin dimer lacks an inversion center, or when the symmetry breaking occurs upon inclusion of magnetostrictive effects, i.e., when polar distortions appear in order to maximize the gain in magnetic energy. Such symmetric exchange-driven electric polarization is usually expected to be large, microscopically arising from non-relativistic Heisenberg-like exchange interactions rather than from spin-orbit coupling. The simplest realization of symmetric magnetostrictive mechanisms has been identified in a frustrated Ising chain system, $Ca_3Co_2MnO_6$, where polarization emerges from Co and Mn cations carrying different charges and undergoing acentric distortions which maximize the magnetic energy gain[22,23]. Similar symmetric-exchange mechanisms have been proposed to explain the multiferroic properties of rare-earth manganites displaying collinear magnetic ordering[24,25].

Although major efforts to achieve significant magnetoelectric coupling were dedicated to bulk inorganic – mostly oxides – compounds, in recent years magnetoelectric effects and spin-electric coupling in organic-based low-dimensional systems have been explored as well, such as the appearance of magnetically induced ferroelectricity in one dimensional organic magnetic chains undergoing spin-Peierls transition[26]. Furthermore, electrical control of magnetic properties in the field of molecular magnets and molecular spintronics is technologically desirable, since it would allow for the manipulation and direct control of the spin state of the molecule at the atomic scale – a crucial issue as long as single molecular magnets are considered – opening new pathways to spin-based quantum information processing[27–31]. In this context, particular attention has been devoted to the possibility of achieving a spin crossover triggered by an electrostatic effect, namely a change of the molecular electronic states in response to a perturbation induced by an electric field[27]. In particular, much work has been devoted to the spin-crossover phenomenon in Fe(II) complexes, where ab initio methods allowed to identify the physical ingredients governing such phenomenon and to explain the hysteresis behavior in terms of microscopic contributions[32–34]. Similarly, Sanvito and collaborators have theoretically explored the possibility of tuning the magnetic exchange coupling in magnetic molecules by an applied electric field, according to a mechanism dubbed electrostatic magnetic-coupling spin crossover effect[29]. Their study shows the feasibility for a family of insulating polar di-cobaltocene-based molecules with super-exchange magnetic interaction to switch the magnetic state with external voltages achievable in two-terminal devices. It is worth to mention that the quest for efficient spin-electric coupling in this field relies on the symmetric-exchange interactions, which are typically more dominant in magnetic materials, rather than the antisymmetric exchange (i.e., the SOC-driven Dzyaloshinskii-Moriya) interaction.

In this context, we have investigated the possible variation of a magnetically induced electric polarization, which would signal an intrinsic magnetoelectric interaction, in two metal-organic one-dimensional compounds based on transition metals (Co and Mn) complexes. The Co-compound of formula $Co(hfac)_2(NITPhOMe)$, known as CoPhOMe in literature, is composed of alternating $Co(hfac)_2$ moieties (where hfac=hexafluoroacetylacetonate) and NITPhOMe (nitronyl-nitroxide) organic radicals arranged in one-dimensional (1D) arrays with a helical acentric structure arising from the trigonal crystallographic lattice[35]. The Mn-compound, denoted as MnPhOMe, is isostructural to CoPhOMe[36]. Although these metal-organic magnetic helices are structurally very similar and are both characterized by an antiferromagnetic (AF) coupling of their magnetic constituents (the transition metal-ions and the ligand radicals), their magnetic properties are remarkably different. As a matter of fact, CoPhOMe is well-known in literature as the first compound where Single-Chain Magnet (SCM) behaviour, i.e., slow relaxation of macroscopic magnetization, has been experimentally observed[35]. At odds with single-molecule magnets, the slow-relaxing magnetization (the magnetic bistability) in SCMs is not exclusively determined by the total magnetic anisotropy, being in fact related to the development of short-ranged spin-spin correlations upon cooling[37–40], pointing to a nontrivial interplay and competition between the magnetic anisotropy and the AF exchange interaction along the chain. On the other hand, MnPhOMe does not show slow relaxation of the magnetization but exhibits a transition to a 3D magnetically ordered phase at low temperature (4.8 K)[36].

Due to their helical structure and their crystallization in an acentric space group, there are no symmetry constraints forbidding the development of an electric polarization or the observation of magnetochiral effects in CoPhOMe and MnPhOMe[41]. Indeed, the interplay between structural chirality and magnetism has been recently studied in details in these systems and a strong magnetochiral dichroism, i.e. different absorption of unpolarised light depending on the magnetic polarization, has been detected for the cobalt derivative by using hard X-rays[42]. Recalling the microscopic mechanisms which have been identified as responsible for the appearance of spin-induced polarization, one immediately realizes that neighbouring spin sites in the considered compounds do not show any inversion center, pointing to possible isotropic exchange-driven polarization. Following our previous work devoted to the investigation of the magnetic properties of CoPhOMe and MnPhOMe[43], we here explore such magnetoelectric interaction for these metal-organic helices by inspecting their electric polarization properties in relation with the magnetic configuration. From a theoretical perspective, by performing density functional theory (DFT) calculations we investigate the electric polarization variation induced by a modification of the chains spin pattern, and hence assess the magnetoelectric coupling. Note that our aim is not to calculate the absolute value of the bulk polarization in the magnetic chains, but rather the changes in polarization induced by a change in their magnetic configurations, so as to focus on the functional form of the magnetoelectric coupling. In this respect, the only meaningful observable is here the difference in electric polarization between the two end states, i.e. the ferrimagnetic (FiM) and the ferromagnetic (FM) one.

The paper is organized as follows. In Sec. 2 a review of the structural and magnetic properties of the systems under investigation is given, and the technical details of the calculations are reported. The results are reported in Sec. 3. Section. 4 summarizes the main findings of the work and closes the article with some general remarks.

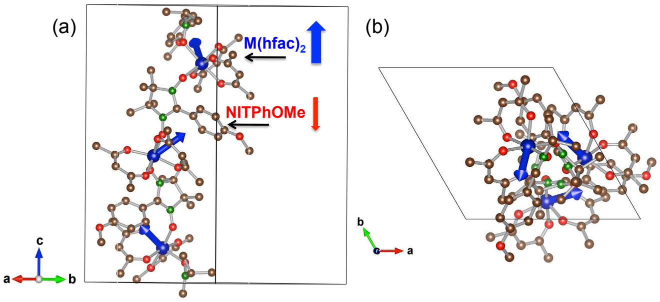

Fig. 1 Crystal structures of isostructural molecular chains CoPhOMe and MnPhOMe: (a) side view ; (b) top view. The M (Co, Mn) atoms are depicted as large blue spheres, and O, N, C atoms are red, green and brown spheres, respectively. For the sake of clarity, F and H atoms are not shown. The metal-organic complexes and organic radicals are highlighted in the side view; the trigonal symmetry of the chains can be seen in the top view. The blue vectors depict the Co-spins directions in the non-collinear spin pattern for CoPhOMe.

2 Systems properties and methodology

The crystal structure of the two chains is shown in Fig. 1. The building blocks are coordination transition-metal complexes M(hfac)$_2$, where M = Co or Mn, linked by nitronyl-nitroxide organic radicals NITPhOMe= 4'-methoxybenzyl-4,4,5,5-tetramethylimidazoline-1-oxyl-3-oxide (denoted also with the shortened term NIT in the following), which crystallize either in the chiral $P3_1$ or $P3_2$ trigonal space groups, forming helical structures. The metal atoms display a distorted octahedral coordination, with the terminating O atoms of the NITs radicals in *cis*-position. The bridging NITs radicals are characterized by two non-equivalent structural patterns for the two moieties bonded to the neighboring M-atoms, labeled as α and β moieties[43].

Regarding the magnetic properties, in CoPhOMe the Co^{2+} ions are in the high-spin state (S=3/2), with electronic configuration $3d^7$, whereas each NIT carries a free electron (S=1/2) that mediates a strong AF-type exchange interaction with the Co ions. The resulting magnetic ground state has a ferrimagnetic (FiM) order, with a total magnetic moment of 6 μ_B per unit cell. The strong exchange coupling in CoPhOMe, together with large easy-axis magnetic anisotropy displayed by the Co^{2+} ions, are the key properties that make this compound a model SCM[35]. Similarly the high-spin Mn^{2+} ions (S=5/2) in MnPhOMe are antiferromagnetically coupled with the NITs, resulting in a FiM magnetic ground state with a total magnetic moment of 12 μ_B per unit cell. Differently from Co-compound, the MnPhOMe comprises isotropic Mn^{2+} ions in the $3d^5$ configuration with negligible magnetic anisotropy, therefore explaining the absence of slow magnetic relaxation effects[36].

First-principles calculations were performed within spin-polarized density functional theory, using the projector-augmented plane-wave (PAW) method[44] as implemented in the VASP materials modelling package[45,46]. The exchange-correlation functional was treated within the generalized gradient approximation (GGA), in the PBE parameterization[47]. Within the PAW potentials scheme, for Co and Mn the $3d4s$ were treated as valence states, while for C, N, O, and F the $2sp$ were considered as valence states. Calculations were performed both in the collinear and non-collinear formalism[48], where spin-orbit coupling has been included for a selected set of calculations. The non-collinear magnetic structures were generated by adopting the constraining technique of the local magnetic moments orientation, as implemented in VASP. A cut-off value of 400 eV was used for the plane-waves basis set, a $2\times2\times1$ mesh of k-points was chosen for the Brillouin-zone integrations, and the convergence criterion for the total energy was set to 10^{-6} eV. The experimental structures were used for the calculations, with lattice parameters $a=b=11.294$ Å, $c=20.570$ Å for the Co chain and $a=b=11.281$ Å, $c=20.846$ Å for the Mn chain. Each unit cell included totally 201 atoms.

The standard local density or generalized gradient approximations of DFT offer a poor description of systems with localized (strongly correlated) orbitals such as $3d$ shells. We have addressed this issue by adopting the GGA+U approach as proposed by Liechtenstein[49], in which the intra-atomic interaction is parameterized in terms of two effective parameters (U, J), where U describes the on-site Coulomb repulsion and J is the on-site exchange correction. We have performed calculations for an extensive set of correlation parameters, comprising three sets of (U, J) values: set a (U_M = 5 eV); set b (U_M = 6.5 eV; J_M = 1.5 eV) *i.e.* an *effective U* as in set a but with the inclusion of a sizable J value, particularly important to properly describe the magnetic anisotropy; set c (U_M = 6.5 eV; J_M = 1.5 eV; U_O=U_N = 6 eV), in which the degree of localization is enhanced by the inclusion of the Hubbard-U term also on p-states of O and N atoms. The electronic polarization properties were calculated via the Berry phase technique[50].

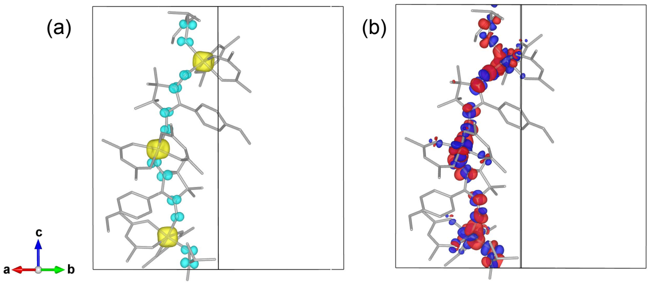

Fig. 2 Exemplified view of the crystal structure of CoPhOMe, with only the bonding frame displayed: (a) isosurface plot of the spin density of the magnetic ground state (FiM), with positive (negative) values depicted in yellow (cyan) color code, evidencing the local AF-type exchange interaction between metal ions and organic radicals; (b) isosurface plot of the charge density difference between the two collinear FiM and FM magnetically ordered states, with positive (negative) charge density depicted in blue (red) color code.

3 Results: spin-induced electric polarization properties

As discussed in our recent work[43], the dominant magnetic interaction in both CoPhOMe and MnPhOMe is antiferromagnetic and occurs between a metal center and the spin of the unpaired electron delocalized on each NIT. This is visually depicted in Fig. 2(a), showing an isosurface of the spin density distribution for CoPhOMe. The positive spin density is localized on Co-sites, yielding each a local magnetic moment of $3\mu_B$, whereas the negative spin density is uniformly distributed on the p-shaped orbitals on the N-O groups of the NITs, yielding overall $1\mu_B$ per connecting radical. Because of the intrinsically delocalized character of the radical unpaired electron and the strength of the magnetic M-NIT interactions, strong charge redistribution effects are expected to occur when the magnetic configuration is modified. Quantum chemistry methods have given major contributions in the theoretical investigation of the intimate mechanisms that govern the exchange interactions between spin bearers with magnetic orbitals of different nature and the resulting charge redistribution[51–54].

In Fig. 2(b), we show the variation of the charge density distribution resulting by switching the ferrimagnetic (FiM) collinear magnetic order to a ferromagnetic (FM) one, where all spins are parallel to the helix axis c. It is evident that the atoms constituting the magnetic path – the metal-ions connected to the O-N-C-N-O atoms of the radicals – are subject to a modulation of the charge distribution by switching the magnetic order, as indicated by the alternating features (positive/negative) of the charge density lobes along the path. Moreover, these compounds have some key structural properties which are required for the magnetoelectric coupling to appear: *i*) the crystals symmetry is chiral and acentric, with a polar axis parallel to the helix direction c, *ii*) the constituent NITs are inversion symmetry-breaking molecules, which are asymmetrically arranged in the cis-coordination with non-equivalent structural patterns, the α and β moieties as discussed above.

All these features call for a detailed investigation of the interplay between magnetic order and electric polarization properties, in order to evaluate whether magnetoelectric coupling effects are present. Based on these general physical considerations, we carried out a detailed investigation of the spin-induced electrical polarization properties of the chains in relation with their magnetic order, as follows. Firstly, we modeled noncollinear magnetic structures by building a set of spin-pattern models along a (continuous) path ideally connecting the two collinear FiM and FM magnetic structures; the changes in polarization are then evaluated as the noncollinear spin-pattern varies along this path (Sec. 3.1). Note that fixed chains structures are here considered, therefore possible magnetostrictive effects are not included in our theoretical analysis, which captures the spin-induced electronic contribution to the polarization as the spin configurations are modulated. Furthermore, we inspected the changes of polarization when parity- and time-reversed structures are considered, unveiling the relationship between structural chirality, magnetism and polarization (Sec. 3.2). We further compare the computed polarization values as evaluated with different choices of (U, J) correlation parameters in GGA+U (Sec. 3.3). Finally, in order to disentangle the single electric dipolar contributions arising from the local switching of the M-NIT magnetic bonds, local electric dipolar terms have been computed for collinear magnetic structures representing single spin-flips for each of the M-ions in the unit cell (Sec. 3.4).

3.1 Polarization properties for noncollinear spin models

The magnetic ground state of CoPhOMe is described by a noncollinear spin-spiral pattern resulting from the two competing terms, the Co-NIT magnetic interactions and the local magnetic anisotropies of the Co^{2+} ions in their specific chemical environments. Experimentally, the orientation of the Co-spins with respect to the helix-axis c has been characterized within the range

$45^\circ - 55^\circ$[55]. We used as starting configuration the spin-spiral model that minimizes the local Co-anisotropies, i.e., with Co-spins aligned along their respective easy-axis directions as shown in Fig. 1, while the spins of the NITs were kept fixed along the helix direction. Specifically, by defining the orientation of the local (Co/NIT) spins in terms of the polar angle θ (with respect to c-axis) and azimuthal angle ϕ (with respect to a-axis), once determined the spin orientation for a Co-site (for Co in site 1 we obtained the values $\theta_{Co,1} = 55.2^\circ$, $\phi_{Co,1} = 255.9^\circ$), the orientation of the spins of the remaining sites in the cell are defined by trigonal lattice symmetry relations ($\theta_{Co,i+1} = \theta_{Co,i}$ and $\phi_{Co,i+1} = \phi_{Co,i} + 120^\circ$ for i spanning the lattice sites 1, 2, 3). The spins of the NITs are aligned along the chain direction ($-c$ axis), i.e., $\theta_{NIT,i} = 180^\circ$ for i=1, 2, 3.

Starting from this spin-spiral configuration, we generated a set of noncollinear spin-models with decreasing and increasing angular opening θ_{Co} along a path ideally connecting the two collinear FiM ($\theta_{Co} = 0^\circ$) and FM ($\theta_{Co} = 180^\circ$) magnetic order states, with a umbrella-like closing and opening movement of the spiral-spin pattern, as sketched graphically in Fig. 3. Accordingly, the polar tilting of the Co-spins with respect to the helix axis was varied in the range 0° – 180° at steps of 30°. As for MnPhOMe, given the nearly isotropic behavior of Mn^{2+} ions, noncollinear magnetic structures were considered with NITs fixed along the $-c$ axis ($\theta_{NIT,i} = 180^\circ$ for i = 1, 2, 3) and Mn-spins lying in the ac-plane and globally rotated from the FiM ($\theta_{Mn,i} = 0^\circ$) to the FM state ($\theta_{Mn,i} = 180^\circ$), coherently for all Mn-spins (for i = 1, 2, 3), as shown schematically in Fig. 4(a).

The variation of the electric polarization along the path of noncollinear magnetic structures connecting the FiM and FM ordered states is shown in Fig. 5. For these calculations the set c of the (U, J) parameters is used, namely the electronic "highly-localized" scenario with the inclusion of correlation also on O and N atoms of the radicals. As a convention, we assigned the collinear starting and ending points of our path to be the polar phases (the FiM magnetic state denoted as P- and the FM as P+), with the nonpolar phase (P_0) corresponding to the noncollinear spin-model with Co - and NIT-spins mutually orthogonal ($\theta_{Co} = 90^\circ$).

As expected, no polarization is allowed to develop in the ab plane due to the crystal trigonal symmetry, while a spin-induced polarization (P_c) appears along the polar (helical) axis c; P_c varies smoothly along the path connecting the FiM to the FM collinear configurations, following a $\sim \cos(\theta_{Co})$ behavior, i.e., proportionally to $\boldsymbol{S}_M \cdot \boldsymbol{S}_{NIT}$. The spin-induced electronic component to polarization is therefore ascribed to an isotropic symmetric-exchange mechanism, with an estimated total variation ΔP_c that amounts to 447 $\mu C/m^2$ (ΔP_c=295 $\mu C/m^2$) for CoPhOMe (MnPhOMe) with the considered set c of (U, J) values. The modulation of c-axis component of the magnetic moment per unit cell along the path is also shown for MnPhOMe, from the FiM ($m_z = 12\ \mu_B$) to the FM ($m_z = -18\ \mu_B$) configuration via the 90° configuration ($m_z = -3\mu_B$) where only NIT spins contribute to the net magnetization.

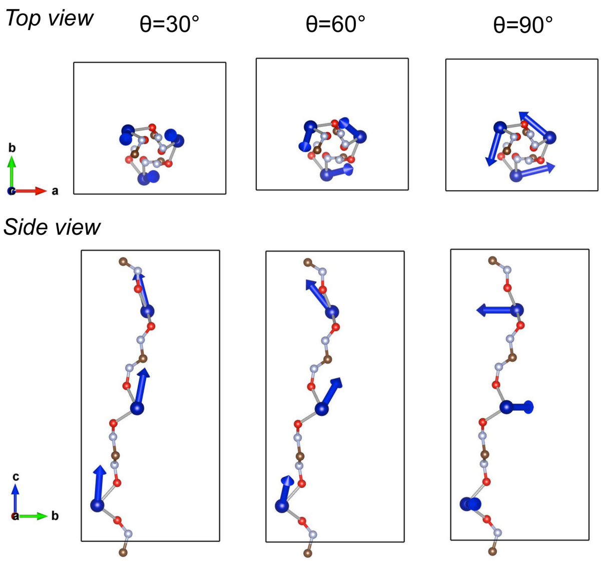

Fig. 3 Spin-spiral magnetic structures modelled for CoPhOMe, at increasing polar angle θ_{Co} from left to right. Only the atoms of the magnetic path – Co and O-N-C-N-O of the NITs – and the Co-spins (in blue) are shown.

In order to check if other spin-induced contributions to polarization may appear, we carried out additional calculations including spin-orbit coupling, finding a tiny variation on top of the symmetric-exchange-like contribution, two orders of magnitude smaller than the main contribution shown in Fig. 5. Furthermore, collinear (FiM and FM) models were also considered by orienting local Co/NIT-spins along the a-axis, resulting in equivalent variations ΔP_c between the two collinear configurations, thus confirming the isotropic nature of the coupling. Finally, we investigated another path of noncollinear spin pattern in MnPhOMe, schematically shown in Fig. 4(b). Here, Mn-spins lying on the plane-ab are rotated, from the collinear configuration ($\Delta\phi_{Mn} = 0^\circ$) at increasing degree of noncollinearity among the Mn-spins at steps of 30°, to the trigonal order ($\Delta\phi_{Mn} = 120^\circ$), with $\Delta\phi_{Mn}$ denoting the relative orientation of Mn-spins in the plane-ab. The NITs-spins are aligned along -c axis ($\theta_{NIT,i} = 180^\circ$ for i = 1, 2, 3). No significant variation of polarization has been observed in this case, P_c remaining fixed to the value obtained in the P_0 configuration; indeed, this is fully consistent with the isotropic symmetric-exchange mechanism, as the Mn-spins are kept orthogonal to the the NIT-spins along the whole path.

Lastly, in the aim of obtaining a more accurate description of the magnetic structure of CoPhOMe, the constrain of collinear NITs-spins aligned along the c axis was removed, and a noncollinear spin-pattern for the NITs was defined based on guess

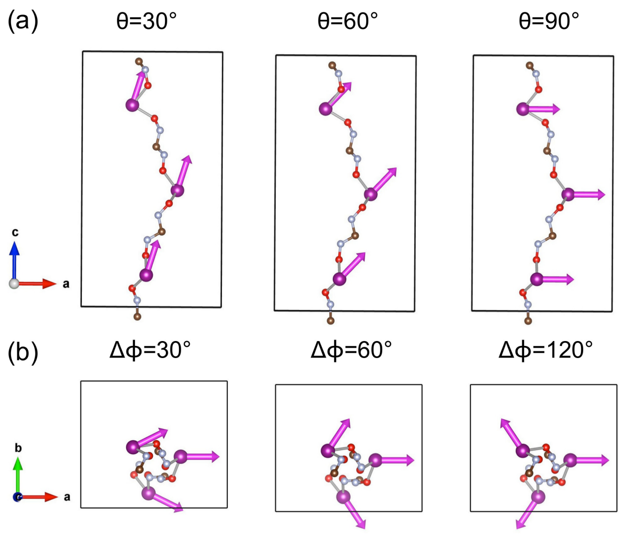

Fig. 4 Spin-patterns modelled for MnPhOMe: (a) Mn-spins coherently rotated on the ac-plane, at increasing polar angle θ (side view). (b) Mn-spins lying on the ab-plane, with increasing degree of non-collinearity among them, defined by the azimuthal angle difference $\Delta\phi_{Mn}$ between neighboring Mn-spins (top view). Only the atoms of the magnetic path – Mn and O-N-C-N-O of the NITs – and the Mn-spins (in purple) are shown.

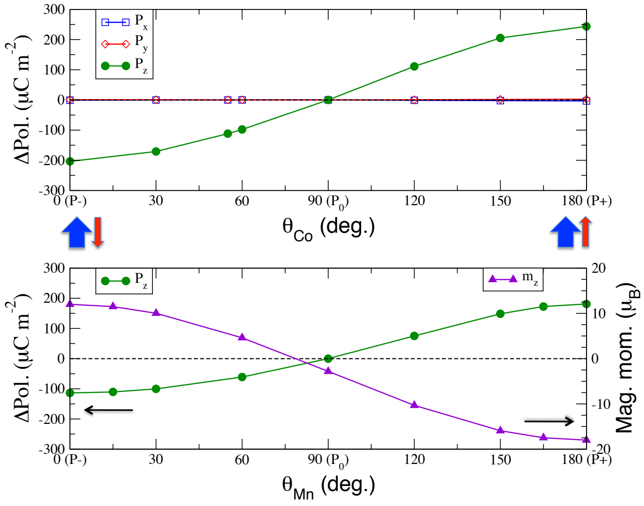

Fig. 5 Polarization response as the noncollinear spin-pattern is varied along an adiabatic path connecting the two collinear FiM (P-) and the FM (P+) magnetic structures, for CoPhOMe (upper panel) and MnPhOMe (lower panel). In the lower panel the modulation of m_z, evaluated as the c-component of the magnetic moment per unit cell, is also shown.

spin configurations that minimize the exchange energy with the neighboring Co-spins. Specifically, the orientation of the NITs-spins was defined as the interpolated one between the adjacent Co-spins, i.e., $\theta_{NIT,i} = \theta_{Co,i}$ and $\phi_{NIT,i} = \phi_{Co,i} + 60°$. Indeed, this magnetic structure is lower in energy compared to the one featuring collinear NITs-spins, and the electric polarization variation profile is shallower than the one shown in Fig. 5, with a halved total polarization response to the magnetic order modulation. This is fully consistent with the proposed mechanism of magnetoelectric coupling because the lower amplitude of polarization modulation is here due to the reduced maximum angular opening between the Co-ions and NITs spin pairs in these spin-pattern models.

3.2 Polarization properties and symmetry relations

We next analyzed the link between the magnetic order driven polarization and symmetry relations, particularly with respect to the time-reversal symmetry and structural chirality. In the previous section we discussed the evolution of the electric polarization along a path with a finite positive magnetization, here our aim is to understand the relationship between the global polarization difference ΔP and the symmetry relations of time-reversal and structural chirality. Since time-reversal symmetry switches the total magnetization of both FiM and FM configurations, we can compare the electric polarization difference between FiM+ and FM+ and that calculated between FiM- and FM-, i.e., ferrimagnetic and ferromagnetic configurations but with opposite magnetization, as realized when time-reversal symmetry is applied to both FiM and FM states individually. For this purpose, we generated two models of CoPhOMe by applying time reversal and parity (inversion) transformation operations to our initial model. The models, as schematically shown in Fig. 6, are obtained by reversing the magnetization direction of both the FiM/FM collinear states (cfr. Fig. 6(b)), and by applying inversion symmetry operation with respect to the cell origin (cfr. Fig. 6(c)).

The results are shown in Fig. 6. We first notice that the global $\Delta P_c = P_c(FM) - P_c(FiM)$ as obtained by noncollinear magnetic calculations (cfr. Sec. 3.1) is consistent with the polarization change between the FiM and FM configurations evaluated from collinear calculations. We find that the polarization response is not changed by magnetization reversal, i.e. equivalent values of polarization change are evaluated for helices with opposite magnetic polarization, whereby the spin-resolved contributions to the polarization are swapped in the two cases (the minority in the majority spin-channel and viceversa). Different is the case for the helix with opposite structural chirality (model (c) in Fig. 6), for which we computed a polarization change which is equivalent in magnitude but reversed along the helix (polar) axis. We then conclude that the magnetic-induced polarization is an even function with respect to time reversal, while it is odd with respect to parity inversion; it follows that enantiomers with different chiral state display opposite polarization contributions. Those enantiomers,

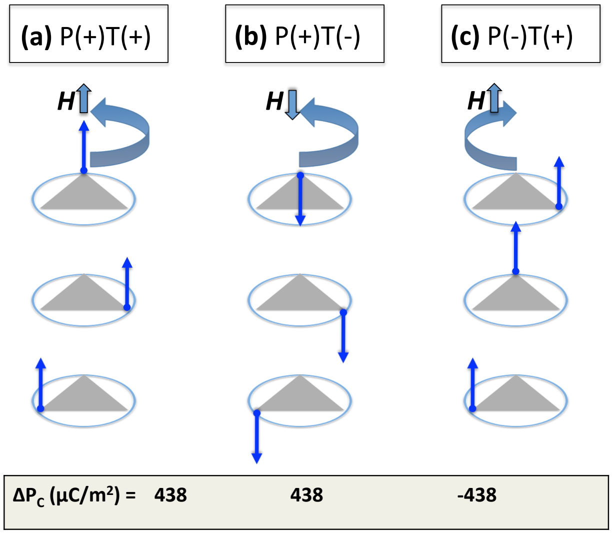

Fig. 6 Schematic of models of CoPhOMe generated by applying time reversal and parity transformations (for simplicity only the Co spins are here displayed): (a) initial model (with positive magnetization), (b) T(-) reversed model (with negative magnetization), (c) P(-) reversed model (opposite chain chirality and positive magnetization). The values of polarization response obtained by going from ferrimagnetic to ferromagnetic hypothetical configurations for the three models are shown.

however, although are iso-energetic structures, unlike standard ferroelectrics, are not connected by an adiabatic path, namely they are not directly switchable by an applied electric field. These results point to an intrinsic structural nature of the phenomenon, where the magnetoelectric coupling is essentially related to the structural arrangements of the interacting magnetic ions and organic radicals in the helical framework.

3.3 Polarization and the role of correlation in GGA+U

In order to further benchmark the predicted spin-induced polarization, we also studied how the polarization response depends on the theoretical treatment of the on-site electronic correlation. Following the methodological approach previously adopted for the first-principles analysis of magnetic properties of the considered compounds[43], we have performed polarization calculations for collinear FiM and FM magnetic structures using the three sets a, b, and c of Hubbard-like (U, J) parameters in GGA+U modeling three degrees of localization. The results of the polarization variation as the FiM magnetic order is switched to FM are reported in Tab. 1, together with the estimates of the exchange couplings of the M-NIT magnetic interactions in the chains. Note that the reported exchange-coupling constants, pertaining to the nearest-neighbor M-NIT interactions, are indeed effective values averaged between the two values obtained accordingly for the two type of metal-radical bonding (α or β) in the compounds[43].

Table 1 Computed polarization variation values along the c axis (right column) obtained by FiM to FM magnetic order switching in CoPhOMe and MnPhOMe, as well as exchange coupling constants (central column) for the dominant M-NIT magnetic interactions. Three different sets of (U, J) parameters in GGA+U have been used: set a (U_M = 5 eV), set b (U_M = 6.5, J_M = 1.5 eV), and set c (U_M = 6.5 eV, J_M = 1.5 eV, U_O = U_N = 6 eV).

CoPhOMe	J_{Co-NIT} (meV)	ΔP$_c$ (μC/m^2)
a	-44.2	1006
b	-38.6	572
c	-29.2	438
MnPhOMe	J_{Mn-NIT} (meV)	ΔP$_c$ (μC/m^2)
a	-48.3	654
b	-48.8	651
c	-40.4	295

The polarization response for CoPhOMe is globally larger than for MnPhOMe, and overall – as expected – a general trend of decreasing polarization response is observed as the degree of correlation is enhanced, moving from set a to c. By using a correlation parameter $U = 5$ eV on the metal ions (set a) we obtain an estimate of polarization variation ΔP$_c$ of about 1000 and 650 μC/m^2 for CoPhOMe and MnPhOMe, respectively. Next, by including a sizeable exchange-parameter J on Co-sites, CoPhOMe displays a marked reduction in ΔP$_c$ (the value is almost halved), whereas a strong reduction in ΔP$_c$ is observed for MnPhOMe when a strong localization is included on the O and N atoms (set c). These findings are consistent with the (purely electronic) symmetric-exchange mechanism, where local electric dipoles are expected to emerge from strong charge redistribution effects between spin sites, which are reduced (alongside with the magnetic exchange interactions) when the degree of correlation is increased.

3.4 Electric dipoles induced by switching local magnetic bonds

A detailed analysis of the nature and magnitude of the magnetoelectric coupling in the magnetic helices has been carried out, showing that only the polarization component along the helices axis develops, due to the trigonal symmetry of the crystals. There are however some relevant aspects that elude this analysis, such as: What is the magnitude of the local electric dipoles contributing to the crystal polarization response? What is their orientation in the crystal? To address these questions, we now focus our attention on the local electric dipoles generated by switching the local magnetic bonds, which are ultimately expected to contribute to the bulk polarization. Physically, we may think of these terms as those that develop at the magnetic domain walls (DWs) between two chain fragments magnetically (FiM) ordered, in which locally an AF-magnetic bond is switched to a frustrated FM-type.

The estimated exchange energies of CoPhOMe were found to be much higher than the (magnetic) anisotropy barrier[43], a strong indication that elementary excitations in CoPhOMe are indeed broad DWs. However, we limited our analysis to modeling sharp DWs because considering the large number of atoms in the unit cell, super-cell calculations would be prohibitive. Yet, there is one more physical reason that justifies this choice. Given the dipolar dependence on the relative orientation of neighboring spins, the modeling of a sharp DW provides essentially the integrated value of the electric dipolar contributions along the path of spins involved into a broad DW.

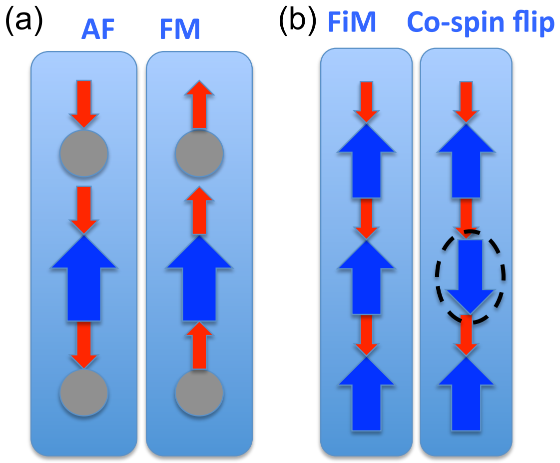

Fig. 7 Models to compute electric dipoles induced by local magnetic switching in the chains. (a) *Method 1*: Local switching of AF-to-FM magnetic bond in Zn-doped chain, with Co-spins (NIT-spins) labelled with thick blue (thin red) arrows, and Zn-sites with grey circles. (b) *Method 2*: Local switching of magnetic bonds via single Co-spin flips.

We devised two independent methods to estimate the local electric dipoles pertaining the smallest chain fragment, which is the spin-trimer comprising a metal ion and the two neighboring NITs radicals. The electric dipole is ideally generated when the AF-type magnetic couplings of the M-NITs spin-trimer are locally frustrated to FM-type. Properly speaking, this local frustration of the magnetic bonds does not describe a sharp DW, but rather a spin excitation in a single FiM domain. As a matter of fact, this single spin-flip excitation comprises two frustrated magnetic bonds whereas a sharp DW is defined by a frustrated bond interposed between two magnetic domains. Therefore, the dipolar contributions produced by DWs would be half of the electric dipole values pertaining to single spin-flip excitations as reported below. *Method 1*. We considered model chains where two (over three) magnetic M sites are replaced by Zn atoms. The diamagnetic Zn^{2+} ions ($3d^{10}$) switch off the magnetic interactions, implying that the only magnetic couplings are those pertaining the spin-trimer formed by the remaining M ion (per unit cell) with the neighboring NITs (see Fig. 7(a)). By building three models of such Zn-doped chains, i. e. $Co_{1/3}Zn_{2/3}$PhOMe and $Mn_{1/3}Zn_{2/3}$PhOMe, in which the magnetic ion (Co or Mn) is located at the three different sites in the unit cell, we were able to estimate the local electric dipoles d_i (for i = 1, 2, 3) resulting from the AF-to-FM local magnetic switching of the spin-trimers at the different sites. *Method 2*. We considered a single M-spin flip in the collinear FiM structures, as shown in Fig. 7(b). By calculating the variation of polarization for the single-spin flip (for each of the magnetic M ions in the cell) with respect to the FiM state, we have estimated the electric dipolar contributions. These polarization calculations have been performed using the set a of the correlation parameters, i.e. a value of $U = 5$ eV on M sites, and finally compared the bulk polarization evaluated as the sum of local electric dipoles with the corresponding ΔP_c values as reported in Tab. 1.

The results for CoPhOMe and MnPhOMe are reported in Tab. 2 and Tab. 3, respectively. The values of the local electric dipoles as determined with the two methods are shown in the upper and lower panels, with computed dipoles magnitudes expressed in Debye (D), and crystal orientations in polar angle θ_{el} (with respect to the c axis) and azimuthal angle ϕ_{el} on the plane-ab (with respect to the a axis). The local electric dipoles d_i generated by AF-to-FM magnetic coupling switching of the spin-trimer in the Zn-doped systems yield a value of $\sim$ 0.49 D for CoPhOMe. The dipoles are tilted with respect to the helix-axis by an average angle θ_{el} of 64.3°, and their orientation on the plane-ab is fully consistent with the three-fold trigonal symmetry of the crystal, as indicated by the negligible deviations ($\Delta\phi_{sym}$) from the phase differences of 120° between neighboring dipoles, imposed by symmetry. The values of the local electric dipoles computed with the two methods are overall comparable within numerical accuracy, with *method 2* yielding slightly larger dipoles in magnitude (by about 3%) and a small difference in the polar tilting (2.5°). The local electric dipoles derived in Zn-doped MnPhOMe chains yield a magnitude of 1.26 D, while those obtained considering magnetic structures of Mn-spin flips have a size of 1.22 D. Despite the amplitude of the electric dipoles is much larger than those evaluated in CoPhOMe, the dipoles d_i are significantly tilted with respect to the helix axis, with an estimated polar angle θ_{el} of about 84° by *method 1* and 81° by *method 2*. Considering the challenging computational task due to the large size of the systems combined with the typically small magnitude of the electronic polarization terms, our computational approach and the comparison between the two complementary methods provides a consistent picture and we can safely argue that the values are within numerical accuracy.

Interestingly, our methodological approach to derive the local electric dipoles reveals that the local contributions are significantly larger in the Mn chain compared to the Co-counterpart by about a factor 2.5, consistently with the larger magnetic exchanges in MnPhOMe. However, the local electric dipoles in MnPhOMe are substantially tilted towards the plane-*ab*, with the resulting effect that the *c* axis component of the electric dipoles, which is lastly the contributing term to the bulk polarization, is larger in CoPhOMe. This is graphically summarized in Fig. 8, where the three local electric dipoles as computed are visualized in the chains, with the convention of metal-sites chosen as vectors' origins. Finally, by summing the local electric dipolar contributions and expressing those values in polarization units (μC/m^2), we are able to directly compare the resulting polarization with the global value obtained by FiM-to-FM magnetic switching in the whole chains. The results, reported in Tab. 4, show indeed a good agreement, further confirming the overall predicted spin-induced electric polarization.

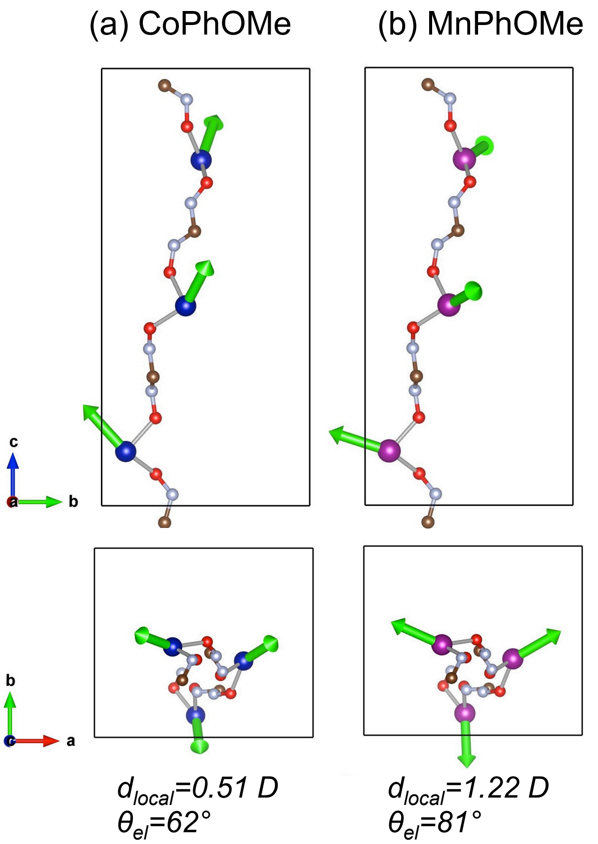

Fig. 8 Electric dipoles induced by local magnetic switching of the M-NITs spin-pairs, as displayed in the chain frame for (a) CoPhOMe and (b) MnPhOMe, with side (top) view in the upper (lower) panel. Magnitude and polar tilting of dipole vectors are also indicated.

4 Conclusions

We have investigated the possible magnetoelectric coupling in chiral metal-organic magnetic chains, showing that an electric polarization is induced by spin-order modulation. Interestingly, by modeling spin-spiral magnetic structures with varying spin polar angle, we find a neat modulation of the electric polarization that varies with the relative alignment of neighbouring metal and radical spins. The functional form of the magnetoelectric coupling has been investigated and found to be compatible with the isotropic symmetric exchange-driven mechanism, being proportional to $\boldsymbol{S}_M \cdot \boldsymbol{S}_{NIT}$ and depending locally on the relative alignment of the spins of the magnetic ions with those of the neighbouring organic radicals. The estimated values of the global ΔP_c by going from ferrimagnetic to ferromagnetic hypothetical configurations are up to ~0.100 μC/cm^2 for CoPhOMe and 0.065 μC/cm^2 for MnPhOMe. The polarization reversal is also achieved when the structural chirality is switched, while it is not observed when time-reversed magnetic ground states are considered (i.e. upon a reversal of the FiM, or spin-spiral, magnetization). To further characterize the local magnetoelectric coupling, we propose a method that allows to quantify the local dipoles that develop in the chains by frustrating local AF-type magnetic bonds. Our results show that the spin-induced local dipoles are indeed quite large (as expected from the symmetry-exchange mechanism) while they partially compensate due to the trigonal symmetry of the chains, resulting in a smaller global polarization along the helices axis. In particular, the local spin-induced electric dipoles are larger in the Mn chain than in the Co complexes, at the same time being more tilted with respect to the polar axis, therefore leading to a smaller global polarization in MnPhOMe as opposed to CoPhOMe. We also verified that the predicted spin-driven polarization does not stem from the relativistic SOC, which contributes only with a tiny correction to the calculated polarization changes.

This observation is in strong contrast with the previously observed magneto-chiral dichroism, which characterizes the cobalt derivative but is practically absent in the more isotropic manganese chain. While X-rays at the metal K edge only probe atomic states, our analysis of the magnetoelectric coupling suggests that NIT radicals play a crucial role in mediating this interaction, being responsible for charge redistribution effects along magnetic bonds which lack an inversion center. The spin density is, in fact, distributed along the path O-N-C-N-O, whose *p*-orbitals are coupled with the *d*-orbitals of the magnetic ions. Due to the strong magnetic interaction, varying the spin configuration steadily change the spin density distribution and the resulting local electric dipoles (a derived integrated quantity). Therefore we can say that the delocalized electron on the NITs, alongside with the cis-coordination of NITs and TM-ions, is a key-property for both the magnetic interaction and the polarization response to a

Table 2 Upper panel: Electric dipoles generated by local switching AF-to-FM of the magnetic coupling in the chain models $Co_{1/3}Zn_{2/3}$PhOMe, where dipole d_i corresponds to Co-atom located at site i (with i =1, 2, 3). Lower panel: Local electric dipoles generated in CoPhOMe by single Co-atom spin flips with respect to the FiM magnetic state. Dipoles magnitudes are expressed in Debye (D), and dipoles orientations in spherical coordinates θ_{el} and ϕ_{el}. $\Delta\phi_{sym}$ is the deviation of the azimuthal angle with respect to perfect trigonal symmetry.

(1) $Co_{1/3}Zn_{2/3}$PhOMe	dipole (D)	θ_{el} (°)	ϕ_{el} (°)	$\Delta\phi_{sym}$ (°)
d_1	0.491	63.91	157.41	-0.27
d_2	0.488	65.00	277.13	0.01
d_3	0.495	64.01	37.14	0.00
(2) Single Co-spin flips	dipole (D)	θ_{el} (°)	ϕ_{el} (°)	$\Delta\phi_{sym}$ (°)
d_1	0.508	61.25	156.69	-0.22
d_2	0.504	62.51	276.37	0.10
d_3	0.511	61.51	36.46	0.00

Table 3 Upper panel: Electric dipoles generated by local switching AF-to-FM of the magnetic coupling in the chain models $Mn_{1/3}Zn_{2/3}$PhOMe, where dipole d_i corresponds to Mn-atom located at site i (with i =1, 2, 3). Lower panel: Local electric dipoles generated in MnPhOMe by single Mn-atom spin flips with respect to the FiM magnetic state. Dipoles magnitudes are expressed in Debye (D), and dipoles orientations in spherical coordinates θ_{el} and ϕ_{el}. $\Delta\phi_{sym}$ is the deviation of the azimuthal angle with respect to perfect trigonal symmetry.

(1) $Mn_{1/3}Zn_{2/3}$PhOMe	dipole (D)	θ_{el} (°)	ϕ_{el} (°)	$\Delta\phi_{sym}$ (°)
d_1	1.2544	84.07	34.53	0.00
d_2	1.2862	84.26	153.55	0.98
d_3	1.2522	84.03	272.77	1.76
(2) Single Mn-spin flips	dipole (D)	θ_{el} (°)	ϕ_{el} (°)	$\Delta\phi_{sym}$ (°)
d_1	1.2110	81.34	33.68	0.00
d_2	1.2390	81.58	152.70	0.99
d_3	1.2078	81.31	272.02	1.66

Table 4 Comparison of the total polarization values for CoPhOMe (upper panel) and MnPhOMe (lower panel) as determined locally (in Zn-doped chains and by single M-spin flips) with respect to the global polarization variations induced by going from FiM to FM hypothetical configurations.

CoPhOMe	ΔP_c ($\mu C/m^2$)
$Co_{1/3}Zn_{2/3}$PhOMe	941
Single Co-spin flips	1058
Chain FiM-to-FM	1006
MnPhOMe	ΔP_c ($\mu C/m^2$)
$Mn_{1/3}Zn_{2/3}$PhOMe	564
Single Mn-spin flips	793
Chain FiM-to-FM	654

magnetic modulation. The values of the polarization estimated for these molecular chains are comparable with those typically observed in oxide-based spin-spiral multiferroics such as $TbMnO_3$ and $TbMn_2O_5$ [19,21], as well as more recently found in molecular multiferroics materials, as shown for instance by Pardo et al.[56] who reported saturation polarization values of 0.070 μC cm^{-2} for a molecular hybrid material combining a 2D oxalate-based bimetallic anion network alternated with polar stacks of cations. An interesting aspect that our study elucidates is that although the global polarization along the polar crystal axis does not exceed 0.100 μC cm^{-2} due to a partial compensation of tilted local dipoles in the trigonal chain structure, the local spin-induced electric dipoles are indeed found to carry sizable dipole moments, pointing to a significative magnetoelectric interaction. Our theoretical prediction opens therefore new perspectives aiming at cross-coupling effects as tools to control the magnetic/electric properties of the considered molecular chains. From an applicative perspective, an interesting effect of modulation and control of magnetic domains by applied external electric fields may stem from the predicted magnetoelectric coupling, similarly to what has been experimentally reported in multiferroics materials[57]. In these chain compounds, however, the focus is on the magnetization dynamics. Specifically, since local electric dipoles variation may originate at the domain walls wherein frustrated magnetic interactions occur, an applied electric field is therefore expected to modify the energetic cost to nucleate a domain wall, hence leading to a modulation of the magnetization dynamics under applied electric fields in single-chain magnets that exhibit this magnetoelectric coupling.

Work supported by Italian MIUR through FIRB project *Nanomagneti molecolari su superfici metalliche e magnetiche per applicazioni nella spintronica molecolare* (RBAP117RWN). We acknowledge the CINECA Award No. HP10B2TGNW (2014), for the availability of high performance computing resources and support. R. S. thanks the support of the European Research Council through the AdG MolNanoMaS (267746).

References

1 I. E. Dzyaloshinskii, *Sov. Phys. JETP*, 1959, **10**, 628.
2 D. N. Astrov, *Sov. Phys. JETP*, 1960, **11**, 708.
3 M. Fiebig, *J. Phys. D: Appl. Phys.*, 2005, **38**, R123.
4 N. A. Spaldin and M. Fiebig, *Science*, 2005, **309**, 391.
5 H. Schmid, *Ferroelectrics*, 1994, **162**, 317.
6 D. I. Khomskii, *Physics*, 2009, **2**, 20.
7 S.-W. Cheong and M. Mostovoy, *Nat. Mater.*, 2007, **6**, 13.
8 Y. Tokura and S. Seki, *Adv. Mater.*, 2010, **22**, 1554.
9 K. F. Wang, J. M. Liu and Z. F. Ren, *Adv. Phys.*, 2009, **58**, 321.
10 A. P. Pyatakov and A. K. Zvezdin, *Phys. Usp.*, 2012, **55**, 557.
11 C. Jia, S. Onoda, N. Nagaosa and J. H. Han, *Phys. Rev. B*, 2006, **74**, 224444.
12 H. Murakawa, Y. Onose, S. Miyahara, N. Furukawa and Y. Tokura, *Phys. Rev. Lett.*, 2010, **105**, 137202.
13 K. Yamauchi, P. Barone and S. Picozzi, *Phys. Rev. B*, 2011, **84**, 165137.
14 C. Jia, S. Onoda, N. Nagaosa and J. H. Han, *Phys. Rev. B*, 2007, **76**, 144424.
15 H. J. Xiang, P. S. Wang, M.-H. Whangbo and X. G. Gong, *Phys. Rev. B*, 2013, **88**, 054404.
16 H. Katsura, N. Nagaosa and A. V. Balatsky, *Phys. Rev. Lett.*, 2005, **95**, 057205.
17 I. A. Sergienko and E. Dagotto, *Phys. Rev. B*, 2006, **73**, 094434.
18 H. J. Xiang, E. J. Kan, Y. Zhang, M.-H. Whangbo and X. G. Gong, *Phys. Rev. Lett.*, 2011, **107**, 157202.
19 T. Kimura, T. Goto, H. Shintani, K. Ishizaka, T. Arima and T. Y., *Nature*, 2003, **426**, 55.
20 M. Kenzelmann, A. B. Harris, S. Jonas, C. Broholm, J. Schefer, S. B. Kim, C. L. Zhang, S.-W. Cheong, O. P. Vajk and J. W. Lynn, *Phys. Rev. Lett.*, 2005, **95**, 087206.
21 T. Kimura, *Annu. Rev. Mater. Res.*, 2007, **37**, 387.
22 Y. J. Choi, H. T. Yi, S. Lee, Q. Huang, V. Kiryukhin and S.-W. Cheong, *Phys. Rev. Lett.*, 2008, **100**, 047601.
23 H. Wu, T. Burnus, Z. Hu, C. Martin, A. Maignan, J. C. Cezar, A. Tanaka, N. B. Brookes, D. I. Khomskii and L. H. Tjeng, *Phys. Rev. Lett.*, 2009, **102**, 026404.
24 I. A. Sergienko, C. Şen and E. Dagotto, *Phys. Rev. Lett.*, 2006, **97**, 227204.
25 S. Picozzi, K. Yamauchi, B. Sanyal, I. A. Sergienko and E. Dagotto, *Phys. Rev. Lett.*, 2007, **99**, 227201.
26 F. Kagawa, S. Horiuchi, M. Tokunaga, J. Fujioka and Y. Tokura, *Nature Phys.*, 2010, **6**, 169.
27 M. Diefenbach and K. S. Kim, *Angew. Chem. Int. Ed.*, 2007, **46**, 7640.
28 M. Trif, F. Troiani, D. Stepanenko and D. Loss, *Phys. Rev. Lett.*, 2008, **101**, 217201.
29 N. Baadji, M. Piacenza, T. Tugsuz, F. Della Sala, G. Maruccio and S. Sanvito, *Nature Mater.*, 2009, **8**, 813.
30 J. Lehmann, A. Gaita-Arino, E. Coronado and D. Loss, *J. Mater. Chem.*, 2009, **19**, 1672.
31 T. Mahfoud, G. Molnár, S. Bonhommeau, S. Cobo, L. Salmon, P. Demont, H. Tokoro, S.-I. Ohkoshi, K. Boukheddaden and A. Bousseksou, *J. Am. Chem. Soc.*, 2009, **131**, 15049.
32 M. Kepenekian, B. Le Guennic and V. Robert, *Phys. Rev. B*, 2009, **79**, 094428.
33 M. Kepenekian, B. Le Guennic and V. Robert, *J. Am. Chem. Soc.*, 2009, **131**, 11498.
34 M. Kepenekian, J. Sanchez Costa, B. Le Guennic, P. Maldivi,

S. Bonnet, J. Reedijk, P. Gamez and V. Robert, *Inorg. Chem.*, 2010, **49**, 11057.

35 A. Caneschi, D. Gatteschi, N. Lalioti, C. Sangregorio, R. Sessoli, G. Venturi, A. Vindigni, A. Rettori, M. G. Pini and M. A. Novak, *Angew. Chem. Int. Ed.*, 2001, **40**, 1760.

36 A. Caneschi, D. Gatteschi, P. Rey and R. Sessoli, *Inorg. Chem.*, 1991, **30**, 3936.

37 C. Coulon, H. Miyasaka and R. Clérac, *Struct. Bond.*, 2006, **122**, 163.

38 L. Bogani, A. A. Caneschi, M. Fedi, D. Gatteschi, M. Massi, M. A. Novak, M. G. Pini, A. Rettori, S. Sessoli and A. Vindigni, *Phys. Rev. Lett.*, 2004, **92**, 207204.

39 C. Coulon, R. Clérac, L. Lecren, W. Wernsdorfer and H. Miyasaka, *Phys. Rev. B*, 2004, **69**, 132408.

40 A. Vindigni, A. Rettori, L. Bogani, A. Caneschi, D. Gatteschi, R. Sessoli and M. A. Novak, *Appl. Phys. Lett.*, 2005, **87**, 073102.

41 D. Szaller, S. Bordács and I. Kézsmárki, *Phys. Rev. B*, 2013, **87**, 014421.

42 R. Sessoli, M.-E. Boulon, A. Caneschi, M. Mannini, L. Poggini, F. Wilhelm and A. Rogalev, *Nature Phys.*, 2015, **11**, 69.

43 M. Scarrozza, A. Vindigni, P. Barone, R. Sessoli and S. Picozzi, *Phys. Rev. B*, 2015, **91**, 144422.

44 P. E. Blöchl, *Phys. Rev. B*, 1994, **50**, 17953.

45 G. Kresse and J. Furthmüller, *Phys. Rev. B*, 1996, **54**, 11169.

46 G. Kresse and D. Joubert, *Phys. Rev. B*, 1999, **59**, 1758.

47 J. P. Perdew, K. Burke and M. Ernzerhof, *Phys. Rev. Lett.*, 1996, **77**, 3865.

48 D. Hobbs, G. Kresse and J. Hafner, *Phys. Rev. B*, 2000, **62**, 11556.

49 A. I. Liechtenstein, V. I. Anisimov and J. Zaanen, *Phys. Rev. B*, 1995, **52**, R5467.

50 R. Resta, *J. Phys. Condens. Matter*, 2000, **12**, R107.

51 J.-B. Rota, C. J. Calzado, C. Train and V. Robert, *J. Chem. Phys.*, 2010, **132**, 154702.

52 O. Oms, J.-B. Rota, L. Norel, C. J. Calzado, H. Rousseliere, C. Train and V. Robert, *Eur. J. Inorg. Chem.*, 2010, **2010**, 5373.

53 M. Verot, J.-B. Rota, M. Kepenekian, B. Le Guennic and V. Robert, *Phys. Chem. Chem. Phys.*, 2011, **13**, 6657.

54 C. Angeli and C. J. Calzado, *J. Chem. Phys.*, 2012, **137**, 034104.

55 A. Caneschi, D. Gatteschi, N. Lalioti, C. Sangregorio, R. Sessoli, G. Venturi, A. Vindigni, A. Rettori, M. G. Pini and M. A. Novak, *Europhys. Lett.*, 2002, **58**, 771.

56 E. Pardo, C. Train, H. Liu, L.-M. Chamoreau, B. Dkhil, K. Boubekeur, F. Lloret, K. Nakatani, H. Tokoro, S.-i. Ohkoshi and M. Verdaguer, *Angew. Chem. Int. Ed.*, 2012, **51**, 8356.

57 T. Zhao, A. Scholl, F. Zavaliche, K. Lee, M. Barry, A. Doran, M. P. Cruz, Y. H. Chu, C. Ederer, N. A. Spaldin, R. R. Das, D. M. Kim, S. H. Baek, C. B. Eom and R. Ramesh, *Nature Mater.*, 2006, **5**, 823.

Table of Contents Entry:

We report first-principles predictions of magnetoelectric coupling in organic magnetic helices and clarify the microscopic mechanism of spin-induced electric polarization.